ISSN 1674-1056
http://cpb.iphy.ac.cn
http://iopscience.iop.org/cpb
中国物理 B
Chinese Physics
中国物理 Chinese Physics B

Experimental and numerical investigation of mid-infrared laser in Pr^{3+}-doped chalcogenide fiber

Hua Chen(陈华), Ke-Lun Xia(夏克伦), Zi-Jun Liu(刘自军), Xun-Si Wang(王训四), Xiang-Hua Zhang(章向华), Yin-Sheng Xu(许银生), Shi-Xun Dai(戴世勋)

Citation: Chin. Phys. B . 2019, 28(2): 024209. **doi:** 10.1088/1674-1056/28/2/024209
Journal homepage: http://cpb.iphy.ac.cn; http://iopscience.iop.org/cpb

What follows is a list of articles you may be interested in

Power of all-fiber amplifier increasing from 1030 W to 2280 W through suppressing mode instability by increasing the seed power

Xue-Xue Luo(罗雪雪), Ru-Mao Tao(陶汝茂), Chen Shi(史尘), Han-Wei Zhang(张汉伟), Xiao-Lin Wang(王小林), Pu Zhou(周朴), Xiao-Jun Xu(许晓军)

Chin. Phys. B . 2019, 28(2): 024208. **doi:** 10.1088/1674-1056/28/2/024208

Mode-locked fiber laser with $MoSe_2$ saturable absorber based on evanescent field

Ren-Li Zhang(张仁栗), Jun Wang(王俊), Xiao-Yan Zhang(张晓艳), Jin-Tian Lin(林锦添), Xia Li(李夏), Pei-Wen Kuan(关珮雯), Yan Zhou(周延), Mei-Song Liao(廖梅松), Wei-Qing Gao(高伟清)

Chin. Phys. B . 2019, 28(1): 014207. **doi:** 10.1088/1674-1056/28/1/014207

Carboxyl graphene oxide solution saturable absorber for femtosecond mode-locked erbium-doped fiber laser

Rui-dong Lv(吕瑞东), Lu Li(李璐), Yong-gang Wang(王勇刚), Zhen-dong Chen(陈振东), Si-cong Liu(刘思聪), Xi Wang(王茜), Jiang Wang(王江), Yong-fang Li(李永放)

Chin. Phys. B . 2018, 27(11): 114214. **doi:** 10.1088/1674-1056/27/11/114214

Femtosecond Tm-Ho co-doped fiber laser using a bulk-structured Bi_2Se_3 topological insulator

Jinho Lee(李珍昊), Ju Han Lee(李周翰)

Chin. Phys. B . 2018, 27(9): 094219. **doi:** 10.1088/1674-1056/27/9/094219

Sb_2Te_3 mode-locked ultrafast fiber laser at 1.93 μm

Jintao Wang(王金涛), Jinde Yin(尹金德), Tingchao He(贺廷超), Peiguang Yan(闫培光)

Chin. Phys. B . 2018, 27(8): 084214. **doi:** 10.1088/1674-1056/27/8/084214

Experimental and numerical investigation of mid-infrared laser in Pr^{3+}-doped chalcogenide fiber*

Hua Chen(陈华)[1,2], Ke-Lun Xia(夏克伦)[1,2], Zi-Jun Liu(刘自军)[1,2,†], Xun-Si Wang(王训四)[1,2], Xiang-Hua Zhang(章向华)[1,3], Yin-Sheng Xu(许银生)[1,2] and Shi-Xun Dai(戴世勋)[1,2]

[1] *Laboratory of Infrared Materials and Devices, Advanced Technology Research Institute, Ningbo University, Ningbo* 315211, *China*
[2] *Key Laboratory of Photoelectric Detection Materials and Devices of Zhejiang Province, Ningbo* 315211, *China*
[3] *Laboratory of Glasses and Ceramics, UMR CNRS* 6226, *University of Rennes* 1, *Rennes Cedex* 135042, *France*

(Received 26 September 2018; revised manuscript received 15 November 2018; published online 10 January 2019)

We report on a chalcogenide glass fiber doped with Pr^{3+} that can be used for commercialized 1.5-μm and 2-μm laser excitations by emitting broadband 3 μm–5.5 μm fluorescence, which is extruded into a preform and then drawn into a step-index fiber. The spectroscopic properties of the fiber and glass are reported, and the mid-infrared fiber lasers are also numerically investigated. Cascade lasing is employed to increase the inversion population of the upper laser level. The particle swarm approach is applied to optimize the fiber laser parameters. The output power can reach 1.28 W at 4.89-μm wavelength, with a pump power of 5 W, excitation wavelength at 2.04 μm, Pr^{3+} ion concentration at 4.22×10^{25} ions/m^3, fiber length at 0.94 m, and fiber background loss at 3 dB/m.

Keywords: mid-infrared fiber laser, chalcogenide glass fiber, rare earth doped glass fiber, laser modelling

PACS: 42.55.Wd, 42.70.Hj, 74.70.Xa **DOI:** 10.1088/1674-1056/28/2/024209

1. Introduction

The broadband optical transmission of chalcogenide glasses in the infrared range offers a wide range of potential applications, such as biological and chemical sensing, nonlinear optics, or optical fibers.[1–5] Notably, selenium-based glasses transmit in the second (3 μm–5 μm) and third (8 μm–12 μm) atmospheric windows. Moreover, selenium glasses, as potential mid-IR laser media, have low phonon energy values and high refractive index values, which result in low probability of de-excitation due to multiphonon relaxation and high absorption/emission cross-section.[6–9] Since 1982, when Reisfeld first reported the spectral characteristics of Er^{3+}-, Nd^{3+}-, and Ho^{3+}-doped Ga–La–S and Al–La–S glasses, many scholars have conducted research on the infrared emission of rare earth-doped chalcogenide glasses.[10] In the near-infrared case, some progress in fiber amplifiers and lasers has been made, including the Nd:1.08-μm continuous fiber laser output and the fiber optic amplification and the optical fiber amplification of Pr^{3+} ions 1.34 μm with a maximum internal gain of 6.8 dB at a pump power of 180 mW.[11,12] However, reports on the mid-infrared cases are mainly concentrated on the fluorescence of glasses and fibers. Studies at home and abroad have shown that although rare earth-doped chalcogenide fibers are the best gain medium for mid-infrared fiber lasers, many problems still remain unsolved, which limits their development and applications. The main problems that stop this technology include the difficulty in manufacturing high-purity rare earth-doped chalcogenide fibers and the self-terminating effect, which makes achieving population inversion difficult.

The Ge–As–Ga–Se (GAGS) glass system has a low tendency to crystallize, high mechanical properties, and high solubility for rare-earth ions. Shiryaev *et al.*[13] provided a new vapor phase transport approach to purify and add the batch of metallic gallium into the silica glass reactor for the GAGS glass synthesis. The content of residual impurities of Se–H can be reduced to 0.023 cm^{-1}. Among the rare-earth dopants, praseodymium is among best to exploit the generation of radiation with 3 μm–5 μm wavelength. However, the upper energy level of Pr^{3+} ion has a long lifetime, which results in a self-terminating effect and makes achieving population inversion difficult. The cascade lasing scheme is an effective solution to depopulate the ($^3F_2$, $^3H_6$) levels and significantly improve the 4.89-μm laser output power.[3,6,14]

In this work, the cascade lasing approach was used to enhance efficiency and was numerically investigated. To obtain realistic results, the $Ge_{10}As_{24}Ga_4Se_{62}$–$Pr_{0.1\ mol\%}$ (GAGS–$Pr_{0.1\ mol\%}$) glasses and fibers were prepared and measured for further calculation and analysis. The emission spectra of the fiber and glass under 2.0-μm laser excitation were then compared. The modeling parameters were directly extracted from

*Project supported by the Young Scientists Fund of the National Natural Science Foundation of China (Grant No. 61605095), the Natural Science Foundation of Zhejiang Province, China (Grant No. LY19F050004), the Natural Science Foundation of Ningbo City (Grant No. 2015A610038), the Open Fund of the Guangdong Engineering Technology Research and Development Center of Special Optical Fiber Materials and Devices (South China University of Technology) (Grant No. 2016-4), and the K C Wong Magna Fund at Ningbo University.

†Corresponding author. E-mail: liuzijun@nbu.edu.cn

© 2019 Chinese Physical Society and IOP Publishing Ltd

the FTIR absorption measurements of the fabricated bulk glass samples using J–O theory and McCumber theory.[15–17] For the proposed laser structures, a numerical model of the three-level fiber laser was developed with the Pr^{3+} doping concentration of 0.1 mol% (4.5×10^{25} ions/m^3), and the dependence of laser performance on fiber length, pump power, doping concentration, and fiber losses were calculated. Moreover, the effect of the idler laser on the influence of the signal laser power was discussed. Finally, to maximize the output power, the fiber laser structural parameters were optimized by using a particle swarm optimization (PSO) algorithm.

2. Numerical model

Figure 1 illustrates the fiber laser cavity composed of two suitable fiber Bragg gratings (FBGs) mirrors. In this model, fiber gratings trapped the idler light at ~ 3.7 μm to promote lasing at ~ 4.89 μm. The reflectivity of the input FBG2/1 for the idler R_1 and signal wavelength R_3 are all 0.95. The output reflectivity was 0.05 for the signal R_4 and 0.95 for the idler wavelength R_2.

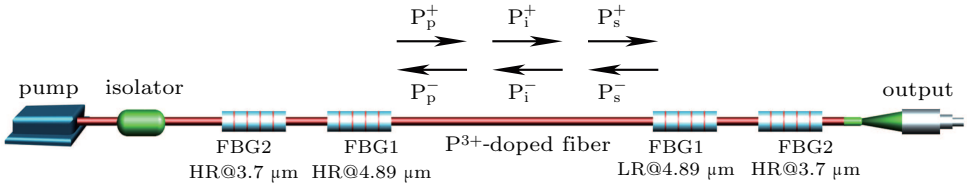


Fig. 1. Schematic illustration of the Pr^{3+}-doped chalcogenide fiber laser cavity.

Figure 2 illustrates the Pr^{3+} ion level diagram by pumping at the wavelength of 2.04 μm. Relevant transitions between the three lowest levels of Pr^{3+} are spontaneous transitions and stimulated emission and absorption transitions between each pair of levels. The rare earth behavior can be modelled as a three-level laser system.

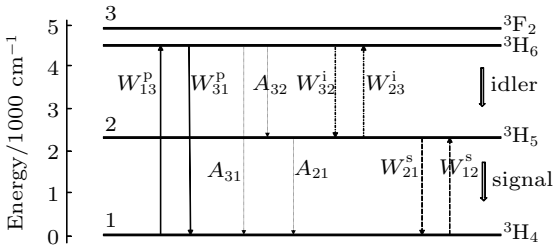


Fig. 2. Three-level model of praseodymium. The most important phenomena are represented (absorption and emission).

Pump light at 2.04 μm is coupled into the Pr^{3+} chalcogenide glass fiber, where it promotes Pr^{3+} ions to the ($^3F_2$, $^3H_6$) (level 3). Moreover, the $^3F_2$ level will be transferred to the $^3H_6$ level through non-radiative transitions quickly due to the multi-phonon relaxation, so that the $^3F_2$ and $^3H_6$ levels can be considered as one level.[18] Transition from this level to the $^3H_5$ (level 2) occurs and is accompanied by fluorescence between 3.3 μm and 4.5 μm. Lasing at a wavelength within this range is obtained using two fiber Bragg gratings (FBG1) tuned to 3.7 μm. Fluorescence from level 2 to the ground state $^3H_4$ (level 1) occurs between 3.8 μm and 5.7 μm, and simultaneous lasing at a wavelength within this range is obtained using two additional fiber Bragg gratings (FBG2) tuned to 4.89 μm.

In steady state, the rate equations can be represented in the following matrix, which forms a set of three algebraic equations:

$$\begin{bmatrix} C_{11} & C_{12} & C_{13} \\ C_{21} & C_{22} & C_{23} \\ 1 & 1 & 1 \end{bmatrix} \begin{bmatrix} N_1 \\ N_2 \\ N_3 \end{bmatrix} = \begin{bmatrix} 0 \\ 0 \\ N_p \end{bmatrix}. \tag{1}$$

The coefficients in the equations are as follows: $C_{11} = W_{13}^p, C_{12} = W_{23}^i, C_{13} = -W_{31}^p - W_{32}^i - 1/\tau_3, C_{21} = W_{12}^s, C_{22} = -W_{21}^s - W_{23}^i - 1/\tau_2, C_{23} = W_{32}^i + \beta_{32}/\tau_3$, where τ_3 and τ_2 are the lifetime of levels 3 and 2, respectively, β_{32} is the branching ratio of transition of levels 3 to 2, N_i with $i = 1, 2, 3$ are the steady-state ion populations of the i-th Pr^{3+} energy level.[19]

The stimulated rates for the pump, signal, and idler are given by

$$W_{ij}^x = \frac{\Gamma_x \sigma_{ij} \lambda_x}{Ahc} P_x, \tag{2}$$

where $x = \mathrm{p}$ represents the pump, s represents the signal, and i represents the idler; Γ_x is the confinement factor; σ_{ij} is the absorption or emission cross-section for the ij transition; and P_x denotes the propagating signal and pump powers, respectively. A is the doping cross-section area, h is Planck's constant, and c is the speed of light in free space.

The laser power propagation equations are as follows:

$$\begin{aligned}
\frac{\mathrm{d}P_\mathrm{p}^+(z)}{\mathrm{d}z} &= -\Gamma_\mathrm{p}\left[\sigma_{\mathrm{ap}}N_1 - \sigma_{\mathrm{ep}}N_3\right]P_\mathrm{p}^+(z) - \alpha_\mathrm{p}P_\mathrm{p}^+(z), \\
\frac{\mathrm{d}P_\mathrm{p}^-(z)}{\mathrm{d}z} &= \Gamma_\mathrm{p}\left[\sigma_{\mathrm{ap}}N_1 - \sigma_{\mathrm{ep}}N_3\right]P_\mathrm{p}^-(z) + \alpha_\mathrm{p}P_\mathrm{p}^-(z), \\
\frac{\mathrm{d}P_\mathrm{i}^+(z)}{\mathrm{d}z} &= -\Gamma_\mathrm{i}\left(\sigma_{\mathrm{ai}}N_2 - \sigma_{\mathrm{ei}}N_3\right)P_\mathrm{i}^+(z) - \alpha_\mathrm{i}P_\mathrm{i}^+(z), \\
\frac{\mathrm{d}P_\mathrm{i}^-(z)}{\mathrm{d}z} &= \Gamma_\mathrm{i}\left(\sigma_{\mathrm{ai}}N_2 - \sigma_{\mathrm{ei}}N_3\right)P_\mathrm{i}^-(z) + \alpha_\mathrm{i}P_\mathrm{i}^-(z), \\
\frac{\mathrm{d}P_\mathrm{s}^+(z)}{\mathrm{d}z} &= -\Gamma_\mathrm{s}\left(\sigma_{\mathrm{as}}N_1 - \sigma_{\mathrm{es}}N_2\right)P_\mathrm{s}^+(z) - \alpha_\mathrm{s}P_\mathrm{s}^+(z), \\
\frac{\mathrm{d}P_\mathrm{s}^-(z)}{\mathrm{d}z} &= \Gamma_\mathrm{s}\left(\sigma_{\mathrm{as}}N_1 - \sigma_{\mathrm{es}}N_2\right)P_\mathrm{s}^-(z) + \alpha_\mathrm{s}P_\mathrm{s}^-(z).
\end{aligned} \tag{3}$$

$P(z) = P^+(z) + P^-(z)$ is the optical mode power (superscript '+' represents the forward propagating beam and superscript '–' represents the backward propagating beam). The coupled equations (1)–(3) were solved self-consistently using the coupled solution method.

3. Experiment and calculation

Figure 3(a) shows the absorption spectra of 0.1-mol% Pr^{3+}:$Ge_{10}As_{24}Ga_4Se_{62}$ glasses. The absorption band at 2.94 μm is assigned to O–H impurity vibrational absorption. The absorption band observed at 4.5 μm is attributed to the ground state electronic absorption band $^3H_5 \rightarrow {}^3H_4$ and also encompasses Se–H extrinsic impurity vibrational absorption.

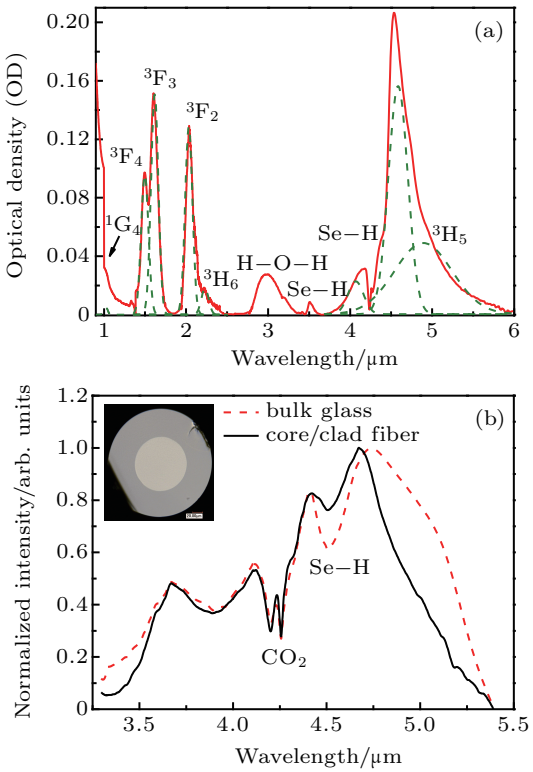


Fig. 3. Absorption spectrum (a) and mid-infrared emission spectral (b) of the 0.1-mol% Pr^{3+}: GAGS glass and fiber.

In the actual calculation, this should be reasonably deducted. Figure 3(b) shows the photoluminescence intensity of the 0.1-mol% Pr^{3+} for bulk and fiber sample together to compare their band shapes. The fiber sample exhibits a greater proportion of its observed emission intensity at wavelengths > 4800 nm compared with the bulk sample. This method is expected due to the longer path length of the fiber sample. For emission in the fiber, the shorter wavelength emission overlaps with the absorption from the ground state ($^3H_5 \rightarrow {}^3H_4$). Therefore, the shorter wavelength emission is self-absorbed and then re-emitted at longer wavelengths. The emission spectra were measured for the calculation of emission cross-sections.

Table 1. Probable radiative electron transitions in Pr^{3+} ions with corresponding wavelengths, spontaneous emission probabilities, A, branching rations β, and the radiative lifetime τ.

Transition		λ/nm	GAGS-$Pr_{0.1\ mol\%}$		
From			A/s^{-1}	β/%	τ/ms
$^3H_5$	$^3H_4$	4890	70.22	100	14.24
$^3H_6$	$^3H_4$	2345	96.76	61.20	6.33
	$^3H_5$	4645	61.33	38.79	
$^3F_2$	$^3H_4$	2039	2614.46	93.12	
	$^3H_5$	3577	192.62	6.86	0.35
	$^3H_6$	14660	0.46	0.02	

The J–O theory can quantitatively calculate the luminous intensity of rare earth ions in a certain precision. The number of spectral absorption bands that have been used in the J–O computations for Pr^{3+} contains six peaks (Fig. 3(a)) centered at 1022, 1478, 1584, 2039, 2345, and 4890 nm.[20,21] To minimize the error, the measured FTIR spectra were corrected by extracting the baseline, each represented by at least 50 selected points. This procedure yielded nine sets of J–O parameters.

Table 2. Parameters used for simulations of Pr^{3+}-doped chalcogenide fiber lasers.

Symbol	Quantity	GAGS-$Pr_{0.1\ mol\%}$	
		Value	Unit
N_{pr}	Pr^{3+} ions concentration	4.5×10^{25}	m^{-3}
A	core radius	5.5	μm
τ_2	lifetime of level 2	14.24	ms
τ_3	lifetime of level 3	6.33	ms
β_{32}	branching ration for 3-2	0.388	
Γ_p	confinement factor for pump	0.034	
Γ_i	confinement factor for idler	0.8	
Γ_s	confinement factor for signal	0.8	
λ_p	pump wavelength	2.04	μm
λ_i	idler wavelength	3.70	μm
λ_s	signal wavelength	4.89	μm
σ_{ap}	pump absorption cross-section	2.32×10^{-24}	m^2
σ_{ep}	pump emission cross-section	0.23×10^{-24}	m^2
σ_{ai}	idler absorption cross-section	0.02×10^{-24}	m^2
σ_{ei}	idler emission cross-section	0.28×10^{-24}	m^2
σ_{as}	signal absorption cross-section	0.53×10^{-24}	m^2
σ_{es}	signal emission cross-section	1.44×10^{-24}	m^2
α_p	fiber loss at pump wavelength	1	dB/m
α_i	fiber loss at idler wavelength	1	dB/m
α_s	fiber loss at signal wavelength	3	dB/m

Radiative transition probabilities (A), branching ratios (β), and radiative lifetime (τ) of the excited states of Pr^{3+} were calculated based on the J–O theory and are summarized in Table 1. Based on these data, the absorption cross sections for each wavelength were calculated, and the emission cross-sections were determined from the measured emission spectra (Fig. 3(b)) and from the spontaneous radiative transition probabilities, A, by using the Füchtbaure–Ladenburg relation, which are all shown in Table 2.

In this modeling, considering the feasibility of the laser's design, the Pr^{3+} concentration 4.5×10^{25} ions/m^3 was selected. The GAGS fiber doped with 4.5×10^{25} ions/m^3 of Pr^{3+} allows to achieve a favorable compromise for easy implementation of fiber drawing, optical attenuation, and fluorescence.[22] The minimum background losses of the GAGS–Pr glass fibers are about 1 dB/m at 2 μm and 4 μm and 3 dB/m at 4.89 μm. To avoid a deleterious nonlinear effect, the maximum pump power is set to 5 W.

4. Results and discussions

Figure 4 shows the optical signal power $P_s(L)$ of the Pr^{3+}-doped fiber laser versus fiber length L for different pump wavelengths. The dopant concentration $N_{Pr} = 4.5 \times 10^{25}$ ions/m^3 and mirror reflectivity ($R_3 = 0.95$, $R_4 = 0.05$) were fixed. Based on the experimental data, Pr^{3+} has strong absorption bands at 1.55 μm and 2.04 μm, and the absorption cross-sections are 1.5×10^{-24} m^2 and 2.32×10^{-24} m^2, respectively. In this study, the detailed calculation of the four-level mode for the 1.55-μm pump was not exhibited. To improve the accuracy of the simulation, the fiber loss values are varied according to the wavelength. The results plotted for a fiber with a background loss of pump and idler wavelengths are 1 dB/m, and the signal wavelength is 3 dB/m. The energy efficiency is higher, and the optimal fiber length is shorter when pumped by 2.04 μm. This result arises because the absorption cross-section at 2.04 μm is larger than that at 1.55 μm. Therefore, in a shorter fiber length, the power of the pump light is absorbed almost completely. In the future, we will further study the difference between the two pump lasers.

Figure 5(a) shows the dependence of output power on the cavity length for different levels of fiber background loss. The maximum output signal power was 1.41 W for 1.28 m cavity length, with fiber loss of 1 dB/m. For fiber loss fixed at 3 dB/m, the maximum output signal power was reduced to 1.07 W for a fiber length of 0.97 m. A rapid decrease of the output power and the optimal fiber length L_{max} was observed with the increase of fiber background loss. A bigger fiber background loss leads to faster pump power depletion and a reduced signal power and short optimal fiber length. To make a more comprehensive analysis of the proposed fiber laser, the influence of background loss on laser performance was investigated. Background loss is a limiting factor that hampers the possibility of achieving mid-IR laser action from selenide-doped fibers. Selenide glass possesses high optical absorption loss at wavelengths around 4.5 μm due to Se–H glass impurities. However, the loss in this spectral region has recently been proven to be reduced to 1.6 dB/m in the host glass by using sophisticated glass purification techniques.[23] The calculated output power as a function of fiber background loss is presented in Fig. 5(b). The mirror reflectivity ($R_3 = 0.95$, $R_4 = 0.05$) was fixed. The output power decreases from 1.33 W to 0.26 W as fiber loss increased from 1 dB/m to 9 dB/m. Output power above 300 mW is expected for a fiber loss < 6 dB/m. Therefore, to obtain efficient laser operation, the fiber loss should be reduced below 6 dB/m.

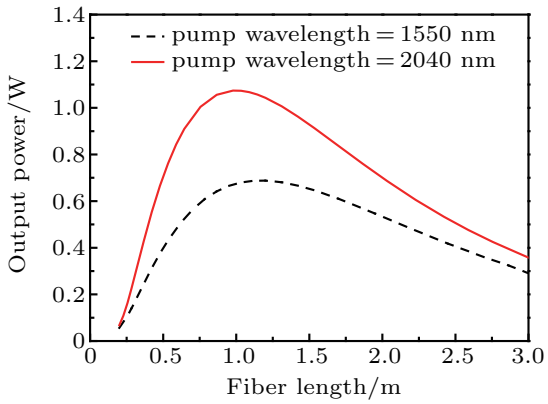


Fig. 4. Calculated signal laser power ($\lambda_s = 4.89$ μm) as a function of fiber length for different pump wavelengths.

Figure 6(a) shows the optical signal power $P_s(L)$ of the Pr^{3+}-doped fiber laser versus length L for different levels of dopant concentration N_{Pr}. In the actual fiber laser design, to get a higher output power, a reasonable fiber length is dependent on the doping concentration. As the doping concentration increases, the optimum fiber length will be shorter, and the maximum output power will be higher. Figure 6(b) shows the optical signal power $P_s(L)$ of the Pr^{3+}-doped fiber laser versus dopant concentration N_{Pr} for different input pump powers. The mirrors reflectivity ($R_3 = 0.95$, $R_4 = 0.05$) were fixed. From Fig. 6(b), we can see that when the doping concentration of rare earth ions exceeds 4.5×10^{25} ions/m^3, the power enhancement is slow due to the limitation of the pump power. Furthermore, the increase in doping concentration causes the homopolar interaction to increase. Because of the concentration quenching in the emission glasses, we chose 4.5×10^{25} ions/m^3 as the optimal concentration.

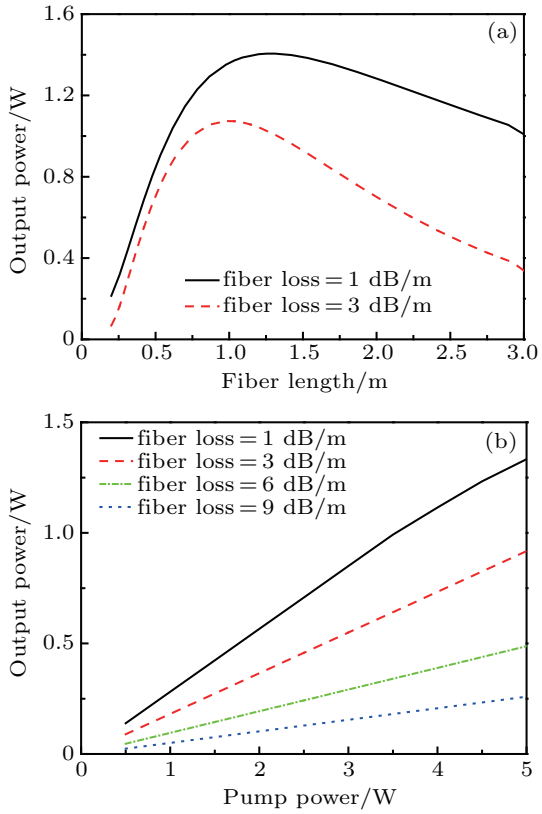


Fig. 5. Optical signal power P_s of the Pr^{3+}-doped fiber laser *versus* the fiber length L for different levels of fiber background loss (a). The signal output power as a function of input pump power for different fiber background losses (b).

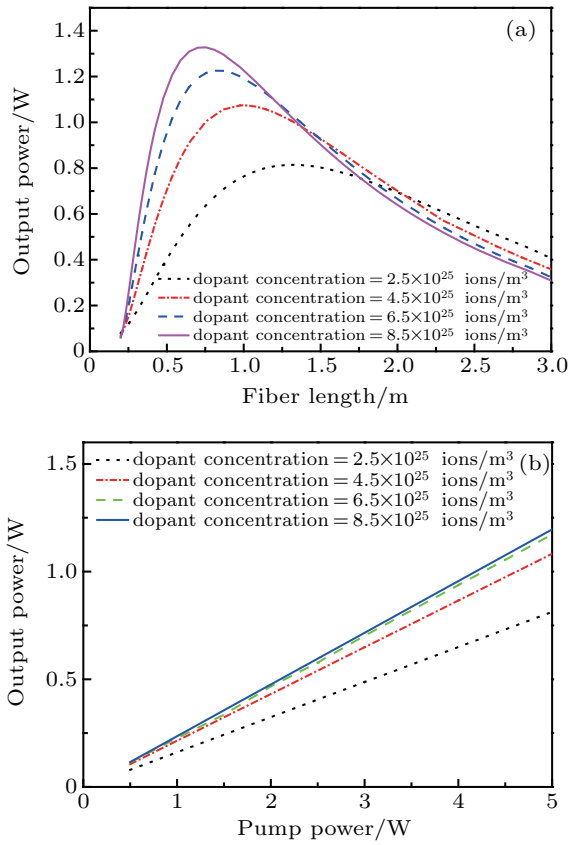


Fig. 6. Optical signal power P_s of the Pr^{3+}-doped fiber laser *versus* fiber length L for different levels of dopant concentration (a). Optical signal power $P_s(L)$ of the Pr^{3+}-doped fiber laser *versus* input pump power for different dopant concentrations (b).

Figure 7(a) shows the optical signal power $P_s(L)$ of the Pr^{3+}-doped fiber laser *versus* output mirror reflectivity R_4 for different pump powers. The results are plotted for a fiber laser with a background loss of 1 dB/m at 2.04 μm and 3.7 μm and 3 dB/m at 4.89 μm. Decreasing the output mirror reflectivity leads to increase in signal output power. The results presented in Fig. 7(a) show that the highest output power can be achieved for an output mirror reflectivity of 0.05 at 4.89 μm. Figure 7(b) shows the optical signal power $P_s(L)$ of the Pr^{3+}-doped fiber laser *versus* fiber length for the idler. Figure 7(a) shows that with the increase of R_4, the output signal power monotonically decreased. According to Fig. 7(b), the existence of idler can effectively improve the signal output power. This result is because the idler laser promotes the de-excitation of the level ($^3F_2$, $^3H_6$) faster. Furthermore, such structure promotes the reabsorption of the idler light and improves the cross-relaxation transition probability between ($^3F_2$, $^3H_6$) $\rightarrow {}^3H_5$, and $^3H_4 \rightarrow {}^3H_5$ in the Pr^{3+} that can effectively enhance the signal power and energy efficiency.[24] This method will reduce the threshold and improve energy conversion efficiency. Therefore, in the actual research, we should consider reducing R_4 and increasing R_2 to increase the laser output power.

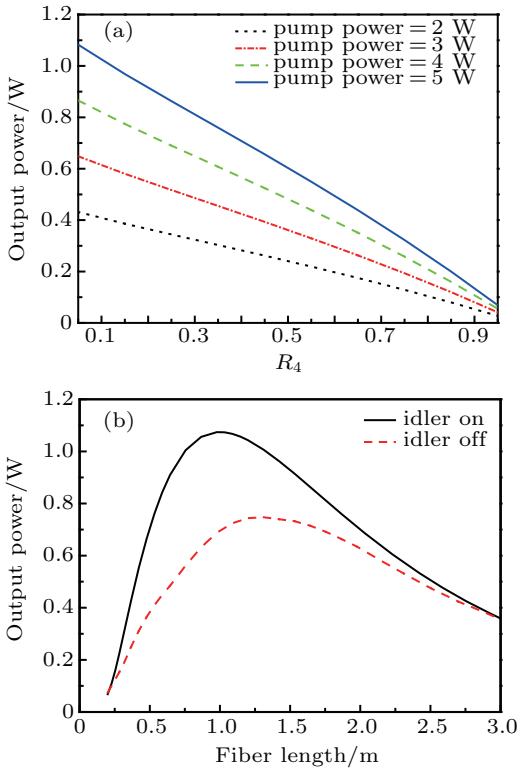


Fig. 7. Optical signal power $P_s(L)$ of the Pr^{3+}-doped fiber laser *versus* output mirror reflectivity R_4 for different pump powers (a). Calculated laser power as a function of fiber length (b). Two cases are considered: without idler and with idler.

The output power of a fiber laser is affected by many parameters that improve the flexibility of the laser design while making the optimization of the laser output power difficult to

accomplish by simple trial and error. In fact, the power of the laser is nonlinearly related to the output mirror reflectivity, fiber length, and dopant concentration. To overcome this problem, the Particle Swarm Optimization (PSO)[25,26] approach is employed to globally optimize the optical source. PSO is a computational method that optimizes a problem by iteratively trying to improve a candidate solution with regard to a given measure of quality, which is a relatively recent heuristic inspired by the choreography of a bird flock. This solves the problem by having a population of candidate solutions, here dubbed particles, and moving these particles around in the search-space according to simple mathematical formulae over the particle's position and velocity. Each particle's movement is influenced by its local best known position and is also guided toward the best known positions in the search-space, which are updated as better positions are found by other particles. This is expected to move the swarm toward the best solutions.

Figure 8(a) shows the effects of fiber length and laser output mirror reflectivity on the output of the laser. The input pump power is $P_{\rm p}(0) = 5$ W, the dopant concentration is $N_{\rm Pr} = 4.50 \times 10^{25}$ ions/m^3, and the mirrors reflectivity is $R_1 = R_2 = R_3 = 95\%$. It allows a quick identification of the best fiber laser configuration via a three-dimensional plot.

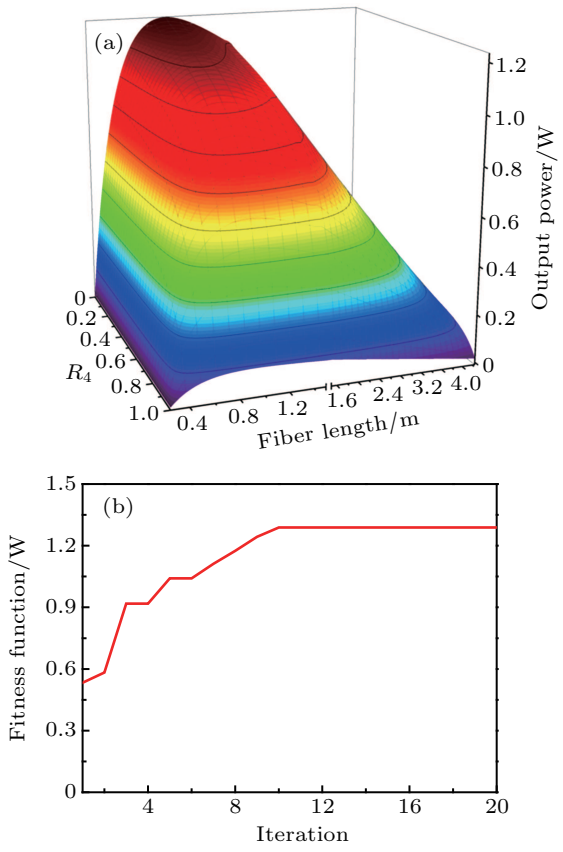


Fig. 8. Output power of the Pr^{3+}-doped fiber laser *versus* laser cavity length L and output mirror reflectivity R_4 (a). Global best fitness value *versus* iteration (b).

Figure 8(b) illustrates PSO fitness function (signal output power) *versus* the iteration number. After iteration for about 10 times, the maximum output power is obtained. The parameters used for optimization are the laser cavity length, output signal reflectivity R_4, and dopant concentration $N_{\rm Pr}$. The input pump power is $P_{\rm p}(0) = 5$ W, and the mirror reflectivity is $R_1 = R_2 = R_3 = 95\%$. The laser output reached 1.28 W, and the energy efficiency can reach 25% with background loss of 3 dB/m. The optimal parameters calculated by the particle swarm method are $L = 0.94$ m, $R_4 = 0.02$, and $N_{\rm Pr} = 4.22 \times 10^{25}$ ions/m^3. These results indicate that chalcogenide glass fiber doped with praseodymium is a good candidate for constructing an efficient fiber laser working in the mid-IR wavelength range.

5. Conclusions

In this paper, a GAGS glass fiber doped with Pr^{3+} has been prepared and studied. We have systematically investigated the dependences of pump wavelengths, cascade structure, and fiber features, and also output mirror reflectivity on the laser's performance. We have demonstrated that three-level fiber lasing is feasible in Pr^{3+}-doped GAGS glass fiber. We observed strong mid-IR emission in the range of 3.5 μm–5.2 μm and a lifetime of 14.24 ms for the $^3H_5 \rightarrow {}^3H_4$ transition. These numerical simulations suggest that the proposed cascade lasing scheme will result in a highly efficient laser compared with a traditional single laser wavelength scheme. The output power function is optimized by the particle swarm optimization algorithm to obtain the maximum output power. Our simulations show that an output signal power of 1.28 W and energy efficiency of 25% at 4.89-μm wavelength can be achieved with $P_{\rm p}(0) = 5$ W, $R_1 = R_2 = R_3 = 95\%$, $L = 0.94$ m, $R_4 = 0.02$, $N_{\rm Pr} = 4.22 \times 10^{25}$ ions/m^3, with fiber loss at 3 dB/m.

References

[1] Sujecki S, Oladeji A, Sojka L, Phillips A, Seddon A B, Benson T M, Sakr H, Tang Z, Furniss D and Scholle K 2014 *International Conference on Numerical Simulation of Optoelectronic Devices*, September 1–4, 2014, Palma de Mallorca, Spain, p. 111
[2] Sakr H, Tang Z, Furniss D, Sojka L, Sujecki S, Benson T M and Seddon A B 2017 *Opt. Mater.* **67** 98
[3] Shaw L B, Cole B, Thielen P A and Sanghera J S 2001 *IEEE J. Quantum Electron.* **37** 1127
[4] Shaw L B, Cole B, Thielen P A, Sanghera J S and Aggarwal I D 2001 *IEEE J. Quantum Electron.* **37** 1127
[5] Yang A P, Qiu J H, Zhang M J, Sun M Y and Yang Z Y 2018 *Chin. Phys. B* **27** 77105
[6] Mescia L, Bia P, De S M, Di T A and Prudenzano F 2012 *Opt. Express* **20** 7616
[7] Oladeji A, Sojka L, Tang Z, Furniss D, Phillips A, Seddon A, Benson T and Sujecki S 2014 *Opt. Quantum Electron.* **46** 593
[8] Seddon A B, Tang Z, Furniss D, Sujecki S and Benson T M 2010 *Opt. Express* **18** 26704
[9] Ren J, Yang G, Zeng H, Zhang X, Yang Y and Chen G 2006 *J. Am. Ceram. Soc.* **89** 2486
[10] Reisfeld R 1982 *Annales De Chimie Science Des Matériaux* **7** 147
[11] Mori A, Ohishi Y, Kanamori T and Sudo S 1997 *Appl. Phys. Lett.* **70** 1230

[12] Samson B N, Schweizer T, Moore R C, Hewak D W and Payne D N 1997 *Conference on Laers and Electron-Optics*, July 14–18, 1997, Chiba, Japan, p. 51
[13] Sójka L, Tang Z, Furniss D, Sakr H, Oladeji A, Bereś-Pawlik E, Dantanarayana H, Faber E, Seddon A B and Benson T M 2014 *Opt. Mater.* **36** 1076
[14] Sakr H, Furniss D, Tang Z, Sojka L, Moneim N A, Barney E, Sujecki S, Benson T M and Seddon A B 2014 *Opt. Express* **22** 21236
[15] Judd B R 1962 *Phys. Rev.* **127** 750
[16] Ofelt G S 1962 *J. Chem. Phys.* **37** 511
[17] Mccumber D E 1964 *Phys. Rev.* **136** A954
[18] Sójka L, Tang Z, Furniss D, Sakr H, Bereś-Pawlik E, Seddon A B, Benson T M and Sujecki S 2017 *Opt. Quantum Electron.* **49** 21
[19] Falconi M C, Palma G, Starecki F, Nazabal V, Troles J, Adam J L, Taccheo S, Ferrari M and Prudenzano F 2017 *J. Lightwave Technol.* **35** 265
[20] Pal I, Agarwal A, Sanghi S and Aggarwal M P 2011 *J. Alloys Compd.* **509** 7625
[21] Sójka Ł, Tang Z, Zhu H, Bereśpawlik E, Furniss D, Seddon A B, Benson T M and Sujecki S 2012 *Opt. Mater. Express* **2** 1632
[22] Pollnau M, Ghisler C, Bunea G, Bunea M, Luthy W and Weber H P 1995 *Appl. Phys. Lett.* **66** 3564
[23] Seddon A B, Furniss D, Sojka L, Churbanov M F, Sujecki S, Benson T M, Shiryaev V S and Tang Z 2015 *Opt. Mater. Express* **5** 1722
[24] Sójka L, Tang Z, Furniss D, Sakr H, Bereś-Pawlik E, Seddon A B, Benson T M and Sujecki S 2017 *Opt. Quantum Electron.* **49** 21
[25] Eberhart and Shi Y 2001 *Proceedings of the* 2001 *Congress on Evolutional Computation*, May 27–30, 2001, Seoul, South Korea, p. 81
[26] Wei H L and Isa N A M 2014 *Inf. Sci.* **280** 111